

Uniwersytet Mikołaja Kopernika w  
Toruniu













Nicolaus Copernicus University

<https://omega.umk.pl>

|  |  |
|--|--|
| Publikacja / Publication   | Measurement and calculation of CO (7–0) overtone line intensities, Balashov Aleksandr, Bielska Katarzyna, Li Gang, Kyuberis Aleksandra A., Wójtewicz Szymon, Domysławska Jolanta, Ciuryło Roman, Zobov Nikolai F., Lisak Daniel, Tennyson Jonathan   |
| DOI wersji wydawcy / Published version DOI                                 | <a href="http://dx.doi.org/10.1063/5.0152996">http://dx.doi.org/10.1063/5.0152996</a>  |
| Adres publikacji w Repozytorium URL /<br>Publication address in Repository | <a href="https://omega.umk.pl/info/article/UMKc1afdfc2c3344d6885ad1d8f9eaf46b7/">https://omega.umk.pl/info/article/UMKc1afdfc2c3344d6885ad1d8f9eaf46b7/</a>  |
| Data opublikowania w Repozytorium /<br>Deposited in Repository on          | 10 lip 2023  |
| Rodzaj licencji / Type of licence  | Uznanie Autorstwa (CC BY)  |
| Cytuj tę wersję / Cite this version  | Balashov Aleksandr, Bielska Katarzyna, Li Gang, Kyuberis Aleksandra A., Wójtewicz Szymon, Domysławska Jolanta, Ciuryło Roman, Zobov Nikolai F., Lisak Daniel, Tennyson Jonathan, Polyansky Oleg L.: Measurement and calculation of CO (7–0) overtone line intensities, Journal of Chemical Physics, American Institute of Physics, vol. 158, nr 23, 2023, Numer artykułu: 234306, s. 1-11, DOI:10.1063/5.0152996 |

RESEARCH ARTICLE | JUNE 21 2023

## Measurement and calculation of CO (7–0) overtone line intensities

Aleksandr A. Balashov ; Katarzyna Bielska ; Gang Li ; Aleksandra A. Kyuberis ;  
Szymon Wójtewicz ; Jolanta Domysławska ; Roman Ciuryło ; Nikolay F. Zobov ; Daniel Lisak ;  
Jonathan Tennyson  ; Oleg L. Polyansky 



*J. Chem. Phys.* 158, 234306 (2023)

<https://doi.org/10.1063/5.0152996>



CrossMark



**The Journal of Chemical Physics**  
**Special Topic: Adhesion and Friction**  
**Submit Today!**



# Measurement and calculation of CO (7-0) overtone line intensities

Cite as: J. Chem. Phys. 158, 234306 (2023); doi: 10.1063/5.0152996

Submitted: 3 April 2023 • Accepted: 31 May 2023 •

Published Online: 21 June 2023



View Online



Export Citation



CrossMark

Aleksandr A. Balashov,<sup>1</sup> Katarzyna Bielska,<sup>1,a)</sup> Gang Li,<sup>2</sup> Aleksandra A. Kyuberis,<sup>3</sup> Szymon Wójtewicz,<sup>1</sup> Jolanta Domysławska,<sup>1</sup> Roman Ciuryło,<sup>1</sup> Nikolay F. Zobov,<sup>4</sup> Daniel Lisak,<sup>1</sup> Jonathan Tennyson,<sup>4,b)</sup> and Oleg L. Polyansky<sup>4</sup>

## AFFILIATIONS

<sup>1</sup>Institute of Physics, Faculty of Physics, Astronomy and Informatics, Nicolaus Copernicus University in Toruń, Grudziadzka 5, 87-100 Toruń, Poland

<sup>2</sup>PTB (Physikalisch-Technische Bundesanstalt), Bundesallee 100, 38116 Braunschweig, Germany

<sup>3</sup>Van Swinderen Institute for Particle Physics and Gravity, University of Groningen, Nijenborgh 4, 9747AG Groningen, The Netherlands

<sup>4</sup>Department of Physics and Astronomy, University College London, Gower Street, London WC1E 6BT, United Kingdom

<sup>a)</sup>Electronic mail: [kbielska@umk.pl](mailto:kbielska@umk.pl)

<sup>b)</sup>Author to whom correspondence should be addressed: [j.tennyson@ucl.ac.uk](mailto:j.tennyson@ucl.ac.uk)

## ABSTRACT

Intensities of 14 lines in the sixth overtone (7-0) band of carbon monoxide ( $^{12}\text{C}^{16}\text{O}$ ) are measured in the visible range between 14 300 and 14 500  $\text{cm}^{-1}$  using a frequency-stabilized cavity ring-down spectrometer. This is the first observation of such a high and weak overtone spectrum of the CO molecule. A theoretical model is constructed and tested based on the use of a high accuracy *ab initio* dipole moment curve and a semi-empirical potential energy curve. Accurate studies of high overtone transitions provide a challenge to both experiment and theory as the lines are very weak: below  $2 \times 10^{-29}$   $\text{cm molecule}^{-1}$  at 296 K. Agreement between theory and experiment within the experimental uncertainty of a few percent is obtained. However, this agreement is only achieved after issues with the stability of the Davidson correction to the multi-reference configuration interaction calculations are addressed.

© 2023 Author(s). All article content, except where otherwise noted, is licensed under a Creative Commons Attribution (CC BY) license (<http://creativecommons.org/licenses/by/4.0/>). <https://doi.org/10.1063/5.0152996>

## I. INTRODUCTION

The carbon monoxide molecule is becoming an important benchmark system for high accuracy absorption line intensity studies.<sup>1-3</sup> From an experimental perspective, the CO molecule has clear advantages due to the ease with which its concentration can be determined and its stability. Since the molecule is diatomic, the absorption lines are well isolated and no line blending or line interference complicates the observations. From the theoretical point of view, the *ab initio* calculation of intensities is facilitated by the relatively small number of electrons and the absence of light (H) atoms, whose presence complicates accurate calculations due to non-adiabatic effects. Furthermore, a diatomic structure means that calculations can be repeated on a fine grid of points and matrix elements determined to high accuracy.<sup>4</sup>

Optical transitions involving relatively highly excited vibrational states of CO are rather difficult to observe. The laboratory

observation of emission overtone hot bands of CO in a  $\text{C}_2\text{H}_2:\text{O}_2$  flame up to band (7-5) was reported in Ref. 5. Earlier observation of the CO band (7-6) was reported in Ref. 6. Four decades later, the first direct laboratory absorption measurements of the high overtone CO (6-0) band were made.<sup>2</sup>

Transitions involving excited vibrational states of CO are important for the interpretation of astrophysical spectra. For example, the (2-0), (3-1), (4-2), (5-3), (6-4), and (7-5) emission CO band heads were seen clearly in the near-infrared spectra of cool stars.<sup>7</sup> Band heads for the (2-0), (3-1), partially (4-2), (5-3), and (7-5) bands were also recorded in the case of another star with the presence of a large amount of gas and dust nearby.<sup>8</sup> Star formation processes were studied for examples of young stellar objects having a emission and absorption features of CO overtone hot band heads in their near-infrared spectra.<sup>9</sup> More recently, the first spatially resolved observations of the CO bandhead emission from

young stellar objects were reported.<sup>10</sup> Other CO hot band heads were observed in the prototype of the EXOr class of young eruptive stars.<sup>11</sup> A compilation of CO overtone band heads, including ones involving the state having vibrational quantum number of  $v = 7$ , can be found online.<sup>12</sup> Finally, highly excited vibrational states, especially those having excitation energy close to one-half of dissociation energy, are very interesting for fundamental studies due to their sensitivity to the proton-to-electron mass ratio.<sup>13</sup>

One of the first sub-percent accuracy line-intensity measurements was made on CO molecules.<sup>1</sup> An example of benchmark studies using the CO spectrum was the recent measurement and first-principles calculation of the (3–0) band line intensities in the near-infrared.<sup>3</sup> This study opened a new era of sub-promille accuracy line-intensity measurements and calculations; such high accuracy was unattainable until recently. However, high-accuracy intensity determinations are much needed for atmospheric studies and meteorological purposes, where, for example, satellite experiments demand transition intensities with sub-percent accuracy.<sup>14</sup>

Sub-percent accuracy for intensities has gradually become achievable and even standard in high-resolution spectroscopy, albeit for important bands of molecules such as CO<sub>2</sub>.<sup>15–17</sup> However, even more challenging is the problem of obtaining sub-percent accuracy for all bands of a given molecule. There are at least two reasons why this goal is topical. One is the fundamental interest in accurate knowledge of molecular spectra and the development of a deep physical understanding of the processes involved. The second reason is for the analysis of the Earth's atmosphere and the atmospheres of the cool stars and exoplanets, which can require sub-promille accuracy for the line intensities of the most important atmospheric absorbers.<sup>18</sup> On the other hand, spectra observed in exoplanets and other astrophysical objects often contain bands such as hot bands, which are weak in the Earth's atmosphere but can become important due to the different physical conditions in these objects.<sup>19</sup>

One of the unsolved problems connected to developing universal models for the band intensities of a given molecule is the accurate measurement and calculation of the highly excited overtone spectra.<sup>20,21</sup> In particular, Medvedev<sup>22</sup> analyzed the nature of the intensities of overtone vibrational transitions and highlighted a number of problems with standard approaches. Subsequent studies<sup>20,21,23–26</sup> highlighted artifacts in calculations of overtone intensities and suggested functional solutions to the form of the dipole moment curve (DMC); more details are given in Sec. III. The calculations of high overtones are much more challenging than those of low overtones in terms of the physical model and numerical calculations precision and accuracy and, thus, high overtones also benchmark calculation quality. In this paper, we develop a solution to this problem based on a study of the previously unobserved CO (7–0) overtone spectrum. In Sec. II, we present the experimental details. In Sec. III, we give the details of the theoretical calculations and present their comparison with the experiment. Our conclusions are presented in Sec. IV.

## II. EXPERIMENT

### A. Measurement details

Intensity measurements for lines in the CO (7–0) band lying between 14 300 and 14 500 cm<sup>-1</sup> were performed using

the frequency-stabilized cavity ring-down spectrometer (FS-CRDS) described in Ref. 27 and references therein. Here, we present only a brief description of the instrument.

The ring-down cavity is nominally 74 cm long, which corresponds to the free spectral range (FSR) of ~203 MHz. For the present measurements, the cavity mirrors are double-wavelength coated and have a nominal intensity reflectivity of ~96% at 1064 nm, corresponding to the Nd:YAG laser wavelength used for cavity length stabilization,<sup>28</sup> and above 99.9988% in the spectral range near 690 nm, corresponding to the probe laser wavelength. This results in a ring-down time decay constant,  $\tau$ , around 206  $\mu$ s in the empty cavity. The probe laser is an ECDL (extended cavity diode laser) emitting in the nominal spectral range between 687 and 707 nm. The probe laser beam is split into several parts. One of the beams is used as a lock beam to tightly lock the laser frequency to the cavity resonant frequency using the Pound–Drever–Hall (PDH) technique,<sup>29</sup> which enables effective, continuous cavity pumping.<sup>30</sup> The other beam, with orthogonal polarization, is detuned from the lock beam by one cavity FSR and serves as an actual probe beam, sampling consecutive cavity modes.<sup>31</sup> Orthogonal polarizations of the probe and lock beams enable their spatial separation outside the ring-down cavity. Another part of the probe's laser beam is used to create an optical beat-note between the probe laser frequency and an optical frequency comb (OFC) to determine the absolute beam frequency at each point in the spectrum.<sup>32</sup> The OFC as well as all frequency generators and counters in the spectrometer are linked to the radio frequency reference, which has a relative stability of  $2 \times 10^{-13}$  at 1 s.<sup>33</sup> The double-wavelength coating of the cavity mirrors enables active stabilization of the cavity length with respect to the iodine-stabilized Nd:YAG laser frequency,<sup>28</sup> which has long-term stability below 5 kHz. Moreover, tuning the reference laser frequency with an acousto-optic modulator in the double pass configuration enables controlled changes of the cavity length and, thus, reduction (fine tuning) of the measurement step below the cavity FSR, which in the measurements presented here was nominally 50 MHz near the line center and one FSR in the line wings.

The cavity temperature was actively stabilized at 296 K and was known with an uncertainty of 35 mK.<sup>27</sup> This uncertainty results from the 30 mK uncertainty due to the temperature sensors, which were calibrated against a Fluke 5641 sensor and an 18 mK temperature gradient along the cavity. The sample pressure was measured with a WIKA/Mensor CPG2500 pressure gauge with a full-scale range of 120 kPa and a nominal accuracy of 0.008%. The comparison with another gauge of the same kind leads to the conclusion that the overall pressure measurement's relative uncertainty is ~0.013%.

We measured 14 lines from the P and R branches of the CO (7–0) band, chosen to be isolated, not overlapped by residual H<sub>2</sub>O and O<sub>2</sub> spectra, and to cover a broad range of rotational quantum numbers. Each of the lines was measured at five pressures in the range from 7 to 100 kPa (stronger lines) or 13–107 kPa (weaker ones). At each pressure, we averaged, typically, 20 scans. We used a commercial sample of CO from Linde Gas with a natural isotopic abundance and purity of 0.99997.

### B. Data analysis

Spectral lines were fitted using a speed-dependent Voigt profile (SDVP),<sup>34</sup> with the speed dependence accounted for using a

quadratic approximation.<sup>35</sup> We used this model because it allows the introduction of additional flexibility to the fitted profile over the ordinary Voigt profile (VP). It allows us to take into account the narrowing effect and possible line asymmetry. It is well known that collisional narrowing of line shape can result from Dicke narrowing<sup>36</sup> as well as speed dependence of collisional width.<sup>34</sup> However, Priem *et al.*<sup>37</sup> showed using a speed-dependent Galatry profile<sup>38</sup> that at low pressures it is very difficult to distinguish between both of these contributions, especially if the signal-to-noise ratio (SNR) does not exceed a few thousand. Similar correlations were subsequently seen<sup>39</sup> using a speed-dependent hard collision model.<sup>40,41</sup> Therefore, we will not try to resolve the nature of line narrowing, and for practical reasons, we will attribute it to speed-dependent narrowing parameters. In this way, we include the narrowing effect to get fits of experimental spectra within the noise and retrieve the proper integrated line area. We note that the SDVP used here is a limiting case of the Hartmann–Tran profile (HTP),<sup>42–44</sup> which originates from a speed-dependent hard collision model<sup>40,41</sup> with the frequency of the velocity-changing collisions and correlation parameters set to zero.

In order to reduce the effect of numerical correlations between line-shape parameters, we used a multispectrum fitting approach.<sup>45–47</sup> The (7–0) band lines of CO have very low transition intensities, below  $2 \times 10^{-29}$  cm molecule<sup>-1</sup>, which limited SNR to 250. In our approach to multispectrum fitting, we enforced linear dependence on the pressure for parameters such as collisional broadening and line shift. In contrast, the values of line-shape parameters that should not change with sample pressure are common

for all pressures for a given line. However, our approach to the line intensity is more complex: initially, to choose the proper line profile, for each sample pressure we independently fit the line area, and then the line intensity is retrieved from a linear fit to the line areas over the sample pressure. This approach provided us with a sensitive test of the applicability of line-shape models to our experimental spectra, independent of the fit residuals. In the case of the VP, our retrieved line intensities depended significantly on sample pressure. However, for SDVP fits, the line intensity remained constant with sample pressure, as expected in our experimental conditions. For this reason, we chose a SDVP for our data analysis, even though, for some of the weaker lines, it does not improve the fit residuals compared to VP fits. The line intensities retrieved from the VP fits are underestimated by between 0.6 and 2% compared to the SDVP results. After choosing the line profile, the final fits were made with line intensities constant with pressure.

Due to very low line intensities, the absorption coefficient in the line peaks has magnitudes of only 0.07–0.6% of the spectral baseline. Sine-like features arising from the etalon effects in our spectrometer are present in the spectral baseline. In contrast to high-SNR spectra, typically achieved in our setup for stronger lines, these features cause significant difficulties during the data analysis as their amplitude is sometimes comparable to the absorption amplitude. The largest etalon in our system is created by reflections between the front and rear sides of the cavity mirrors. Both cavity mirrors are placed inside the thermally stabilized cavity, but other surfaces parallel to the mirrors, such as the photodetector surface and beam

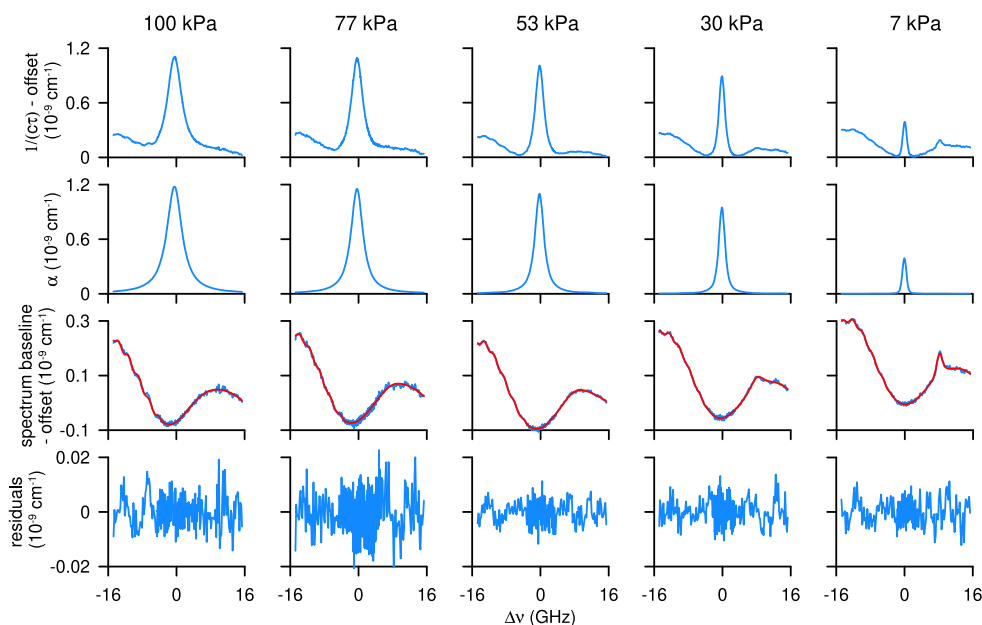


**FIG. 1.** CO (7–0) band P9 line measured using a CRDS technique at 5 pressures, as indicated at the top, and a temperature of 296 K. In the top row, raw spectra are presented and shifted vertically for clarity. The second row plots the fitted CO line profile at the given pressure. The third row plots the spectral baseline shifted by the same offset as the top row: the red curve is the baseline model, and in blue, the actual baseline is shown. For the P9 line, the spectral baseline model additionally includes one water vapor line, which lies  $\sim 8$  GHz away from the CO line and is clearly visible at the lowest pressure. The bottom row shows the fit residuals. On the horizontal axis, the frequency detuning from the unperturbed line position is given. The vertical offsets applied for raw spectra and baseline plots, starting from the highest pressure, are  $206 \times 10^{-9}$  cm<sup>-1</sup>,  $193.2 \times 10^{-9}$  cm<sup>-1</sup>,  $180.4 \times 10^{-9}$  cm<sup>-1</sup>,  $167.55 \times 10^{-9}$  cm<sup>-1</sup>, and  $154.7 \times 10^{-9}$  cm<sup>-1</sup>, respectively.

**TABLE I.** Uncertainty budget for the line intensities. All components are given as standard uncertainties ( $1\sigma$ ).

| Uncertainty component                     | Range (%) |
|---|-----------|
| Type A                                    | 0.2–2     |
| Contributions to B type uncertainty       |           |
| Choice of multispectrum fitting procedure | 1–16      |
| Baseline model uncertainty                | 2.2–13    |
| Choice of line profile                    | 0.6–2     |
| Long-term repeatability                   | 2         |
| Frequency reference accuracy              | <0.1      |
| Temperature measurement                   | <0.1      |
| Temperature dependency                    | <0.1      |
| Pressure measurement                      | <0.1      |
| Total uncertainty                         | 3.3–21    |

spliters, are located outside the thermal enclosure. Corresponding etalons change their parameters during the data acquisition, which typically lasts 9 h per pressure. Therefore, in some cases, the etaloning effect on our spectra cannot be fully accounted for. However, we simulated its effect on the spectra, and its possibly unaccounted effect on the line intensity is included in the uncertainty estimation. The spectral baseline model, for a given pressure, consists of constant cavity losses corresponding to the absorption-free case together with a small linear slope to account for the mirrors' reflectivity change with wavelength and up to three etalons modeled with sine functions. For some of the lines, the model also includes blending with water vapor or oxygen B-band transitions, as both of these gases are present in our system in residual amounts. For example, Fig. 1 shows spectra acquired for the P9 line, together with the spectral baseline model and fit residuals, where an undesirable water line and residual etaloning effect are noticeable.

The total relative standard uncertainty of the line intensity is between 3.3% and 21% for the strongest and weakest lines, respectively, and its components are given in Table I. It consists of type A uncertainty, arising from the fit uncertainty, and type B uncertainty. Type B uncertainty has several components: the most significant ones arise from the baseline model uncertainty, the choice of the line profile model, and the difference between fits assuming different approaches to line intensity determination described above. The measurement repeatability (after two months) adds a relative uncertainty of 2%. Other contributions to the type B uncertainty are

the pressure and temperature measurement uncertainties, the temperature dependency of the line intensity, and frequency reference accuracy, of which none exceeds 0.1%.

### III. THEORETICAL CALCULATIONS AND COMPARISON WITH EXPERIMENT

The accuracy of intensity calculations (both purely *ab initio* and semi-empirical) is determined by the accuracy of the wavefunctions and dipole moment curve (DMC), where the uncertainty in the wavefunctions depends on the potential energy curve (PEC) and solution of the nuclear-motion Schrödinger equation. Here, we used an empirical PEC from Coxon and Hajigeorgiou,<sup>48,49</sup> which reproduces the CO transition frequencies within experimental uncertainty. DMCs were computed *ab initio* using the electronic structure package MOLPRO<sup>50</sup> (Version 2020.1 linked October 6, 2020) at the multi-reference configuration interaction (MRCI) level of theory with a Davidson correction (+Q)<sup>51</sup> using an aug-cc-pCV6Z basis set. The Davidson or similar Pople corrections are perturbative corrections added to allow for high-order correlation terms not allowed for in the MRCI model. Dipoles were calculated using finite differences and an electric field of 0.0002 a.u.

A natural first choice for the complete active space (CAS) for the DMC calculations was to use the same level of *ab initio* theory that gave sub-promille accuracy for the (3–0) band in our previous study.<sup>3</sup> Therefore, DMC computed using a (7220) CAS (see MOLPRO description<sup>50</sup>) was initially used to calculate line intensities for the (7–0) and (6–0) bands lines. However, this attempt to calculate the intensity of (6–0) lines resulted in a three-order-of-magnitude discrepancy with the known experimental results.<sup>2</sup> We, therefore, tested the (6220) CAS DMC calculated previously, as this DMC gave reasonable agreement for the (6–0) band.<sup>3</sup> Using the (6220) CAS gave us excellent results (see Table II) for the (6–0) band, as expected. The calculated (7–0) line intensities using this CAS (see Table III) result in reasonable line intensities, which differ from the HITRAN prediction<sup>52</sup> for the (7–0) band by tens of %, unlike the (7220) CAS results. Comparing with the (7–0) intensity measurements once they became available shows that our calculations give results almost, but not quite, within the experimental uncertainties; see the DF 0.05 and DR 0.05 columns of Table III, where DF and DR denote Davidson fixed and Davidson relaxed corrections, respectively.

Following this, we increased the density twofold so that the distance between the points became  $0.025 a_0$  instead of  $0.05 a_0$ . The results are presented in the DF 0.025 and DR 0.025

**TABLE II.** Comparison of experimental line intensities with those calculated using different models for the (6–0) band of CO. Intensities,  $S$ , are based on the reference temperature  $T = 296$  K and scaled to 100% relative abundance of the  $^{12}\text{C}^{16}\text{O}$  isotopologue using the HITRAN-based natural abundance of 0.986 544. The line wavenumbers and intensities are from Ref. 2. All calculations used a complete active space of (6220) and an aug-cc-pCV6Z basis set. DF and DR denote Davidson's fixed and relaxed corrections.

| Line | Wavenumber ( $\text{cm}^{-1}$ ) | $S$ ( $\text{cm molecule}^{-1}$ ) | DF O–C (%) | DR O–C (%) |
|------|---------------------------------|-----------------------------------|------------|------------|
| R5   | 12 482.423 74                   | $9.30 \times 10^{-29}$            | –1.3       | –0.7       |
| R7   | 12 486.956 65                   | $9.33 \times 10^{-29}$            | –0.2       | 0.4        |
| R9   | 12 490.644 87                   | $7.85 \times 10^{-29}$            | –2.6       | –1.8       |
| R10  | 12 492.171 85                   | $7.04 \times 10^{-29}$            | –1.5       | –0.6       |

**TABLE III.** Comparison of experimental line intensities measured in this work with those calculated with different models for the (7–0) band of CO. Intensities,  $S$ , are based on the reference temperature  $T = 296$  K and given for natural isotopic abundance. All calculations used a complete active space of (6220) and an aug-cc-pCV6Z basis, apart from the final column, which uses the (7220) CAS. DF and DR denote Davidson's fixed and relaxed corrections. 0.05 and 0.025 mean a grid spacing of  $0.05 a_0$  and  $0.025 a_0$ , respectively. O–C denotes relative differences between observed (experimental) and calculated line intensities. The last column, fit.ai0125 DMC, used a DMC obtained from dipoles computed with a  $0.0125 a_0$  step size and a (7229) CAS. The line wavenumbers are from HITRAN.

| Line | Wavenumber<br>( $\text{cm}^{-1}$ ) | $S$ exp.<br>( $\text{cm molecule}^{-1}$ ) | Exp. uncert.<br>(%) | DF 0.05<br>O–C (%) | DF 0.025<br>O–C (%) | DR 0.05<br>O–C (%) | DR 0.025<br>O–C (%) | Medvedev and<br>Ushakov <sup>26</sup> O–C (%) | fit.ai0125<br>O–C (%) |
|------|------------------------------------|---|---------------------|--------------------|---------------------|--------------------|---------------------|---|-----------------------|
| P19  | 14 334.401 63                      | $1.807 \times 10^{-30}$                   | 21                  | 12                 | 37                  | –10                | 13                  | 17  | 10.3                  |
| P16  | 14 358.363 21                      | $3.645 \times 10^{-30}$                   | 7.4                 | 3                  | 25                  | –18                | 2                   | 6   | 0.0                   |
| P13  | 14 380.141 03                      | $6.698 \times 10^{-30}$                   | 4.1                 | 6                  | 27                  | –16                | 4                   | 8   | 1.2                   |
| P12  | 14 386.914 36                      | $7.530 \times 10^{-30}$                   | 4.0                 | 3                  | 23                  | –18                | 0                   | 4   | –2.2                  |
| P11  | 14 393.444 46                      | $9.067 \times 10^{-30}$                   | 4.1                 | 10                 | 31                  | –13                | 7                   | 11  | 4.0                   |
| P10  | 14 399.731 19                      | $9.592 \times 10^{-30}$                   | 3.7                 | 6                  | 25                  | –17                | 2                   | 6   | –0.3                  |
| P9   | 14 405.774 42                      | $1.065 \times 10^{-29}$                   | 3.3                 | 10                 | 31                  | –13                | 7                   | 10  | 3.4                   |
| P8   | 14 411.573 98                      | $1.099 \times 10^{-29}$                   | 3.4                 | 9                  | 30                  | –14                | 5                   | 10  | 2.7                   |
| P7   | 14 417.129 75                      | $1.103 \times 10^{-29}$                   | 3.4                 | 10                 | 29                  | –14                | 5                   | 10  | 2.7                   |
| P4   | 14 432.332 75                      | $8.445 \times 10^{-30}$                   | 3.8                 | 10                 | 30                  | –14                | 5                   | 9   | 2.2                   |
| P1   | 14 445.336 24                      | $2.543 \times 10^{-30}$                   | 11                  | 17                 | 38                  | –9                 | 11                  | 16  | 8.2                   |
| R0   | 14 452.781 33                      | $2.462 \times 10^{-30}$                   | 12                  | 14                 | 35                  | –11                | 9                   | 13  | 5.6                   |
| R4   | 14 464.728 85                      | $9.119 \times 10^{-30}$                   | 3.5                 | 8                  | 29                  | –17                | 3                   | 7   | –0.2                  |
| R6   | 14 469.228 92                      | $9.988 \times 10^{-30}$                   | 3.5                 | 6                  | 28                  | –18                | 2                   | 6   | –1.3                  |

**TABLE IV.** Comparison of experimental and (7220) CAS model calculated line intensities in the (7–0) band of CO. Intensities,  $S$ , are based on the reference temperature  $T = 296$  K and natural isotopic abundance, and (7–0) band intensities are measured in this paper; (5–0) band intensities are from HITRAN; and (6–0) band intensities are from Ref. 2. The line wavenumbers are from HITRAN.

| Band | Line          | Wavenumber ( $\text{cm}^{-1}$ ) | $S$ exp. ( $\text{cm molecule}^{-1}$ ) | exp. uncert. (%) | DF 0.05 O–C (%) | DF 0.025 O–C (%) |
|------|---------------|---------------------------------|--|------------------|-----------------|------------------|
| 7–0  | P19           | 14 334.401 63                   | $1.81 \times 10^{-30}$                 | 21               | 1767            | 117              |
|      | P16           | 14 358.363 21                   | $3.65 \times 10^{-30}$                 | 7.4              | 1808            | 70               |
|      | P13           | 14 380.141 03                   | $6.70 \times 10^{-30}$                 | 4.1              | 1985            | 56               |
|      | P12           | 14 386.914 36                   | $7.53 \times 10^{-30}$                 | 4.0              | 1945            | 46               |
|      | P11           | 14 393.444 46                   | $9.07 \times 10^{-30}$                 | 4.1              | 2092            | 52               |
|      | P10           | 14 399.731 19                   | $9.59 \times 10^{-30}$                 | 3.7              | 2003            | 42               |
|      | P9            | 14 405.774 42                   | $1.07 \times 10^{-29}$                 | 3.3              | 2077            | 45               |
|      | P8            | 14 411.573 98                   | $1.10 \times 10^{-29}$                 | 3.4              | 2026            | 41               |
|      | P7            | 14 417.129 75                   | $1.10 \times 10^{-29}$                 | 3.4              | 1975            | 38               |
|      | P4            | 14 432.332 75                   | $8.45 \times 10^{-30}$                 | 3.8              | 1761            | 34               |
|      | P1            | 14 445.336 24                   | $2.54 \times 10^{-30}$                 | 11               | 1562            | 40               |
|      | R0            | 14 452.781 33                   | $2.46 \times 10^{-30}$                 | 12               | 1308            | 38               |
|      | R4            | 14 464.728 85                   | $9.12 \times 10^{-30}$                 | 3.5              | 850             | 37               |
| R6   | 14 469.228 92 | $9.99 \times 10^{-30}$          | 3.5                                    | 679              | 42              |                  |
| 5–0  | P10           | 10 405.920 99                   | $3.14 \times 10^{-28}$                 |                  | 64              | 25               |
|      | P5            | 10 431.249 90                   | $2.34 \times 10^{-28}$                 |                  | 88              | 34               |
|      | R0            | 10 455.892 17                   | $3.57 \times 10^{-29}$                 |                  | 144             | 45               |
| 6–0  | R5            | 12 482.423 74                   | $9.17 \times 10^{-29}$                 |                  | 2733            | 1489             |
|      | R7            | 12 486.956 65                   | $9.20 \times 10^{-29}$                 |                  | 3522            | 1837             |
|      | R9            | 12 490.644 87                   | $7.74 \times 10^{-29}$                 |                  | 4582            | 2270             |
|      | R10           | 12 492.171 85                   | $6.95 \times 10^{-29}$                 |                  | 5476            | 2637             |

columns of Table III; the use of the finer grid gives a significant further improvement. All the observed – calculated (O–C) residues for DR 0.025 are less than the two experimental standard uncertainties (see Table IV) and are better than the results obtained using the empirically-determined DMC of Medvedev and Ushakov.<sup>26</sup>

However, a full *ab initio* solution should achieve experimental accuracy using a single DMC for all bands; such universally accurate results are not reached by these calculations, as good results are obtained using the (6220) CAS and not the (7220) CAS, which gave excellent results for the (3–0) band.<sup>3</sup> In Subsection III A, we describe our attempts to achieve good results for all bands and to understand the problems that give rise to the extravagantly large discrepancies given by the (7220) CAS for the (7–0) band.

### A. Comparison of different models

Initial studies of highly accurate (sub-percent or better) first principles line intensities calculations<sup>15,16</sup> focused on accurate calculations for a single band. This was because intensity measurements with sub-percent or better accuracy were only available for single bands. There was an implicit supposition that the accuracy obtainable using the first principles calculations for other bands should be similarly accurate. This supposition turned out to be incorrect.<sup>53</sup> A challenging goal of accurate line intensity calculations is to compute accurate intensities for all bands for which CO provides a natural

benchmark. In this section, we describe our attempts to obtain a global *ab initio* model.

First, we need to understand why the (7220) CAS calculations, which give line intensities for the fundamental and first three overtone bands within experimental accuracy, perform so poorly for the (7–0) band. Tests performed with the (6220) CAS DMC pointed toward a reason for the discrepancy. When we doubled the density of the points, the deviation from the experimental measurements improved from 2000% to 50% for the (7220) CAS calculation, a much more significant improvement than the one found for the (6220) CAS calculation. We, therefore, tested the use of an even denser grid of *ab initio* points, but it became apparent that a simple increase in the density of points does not lead to convergence to an accurate solution. A search for possible problematic *ab initio* points was, therefore, initiated. In order to find them, we interpolated our 25 and 50 point sets. The 100 interpolated points obtained were compared with the set of 100 *ab initio* points. As shown in Fig. 2(a), this comparison identified three intervals containing problematic points as well as two distinct anomalous points. These points clearly affected the accuracy of our results; for example, the removal of just one of the distinct anomalous points resulted in immediate improvements in the predicted intensities of some lines by a factor of five or more.

As Fig. 2(a) shows, the interpolated dipole moments differ from the *ab initio* values the most in the three regions marked with red boxes, with the largest difference of  $1.65 \times 10^{-6} e \cdot a_0$  in the first window. In comparison, in the stable regions such as from 2.2 to 2.375  $a_0$ , the largest difference is only  $9.74 \times 10^{-8} e \cdot a_0$  at 2.125  $a_0$ , as shown in Fig. 2(b). The fluctuations in the marked regions are smaller than the differences associated with the choice of CAS. However, they generate dramatically larger differences in the calculated line intensities for higher overtone bands, for example, resulting in calculated intensities 40-fold larger than those measured for the (6–0) band. Figure 2(c) shows a major outlier of  $-4.5 \times 10^{-5} e \cdot a_0$  at 2.185  $a_0$ .

We, therefore, decided to remove all the problematic points and look at the influence of this action on the intensities. The last but one column of Table V shows that this results in a significant improvement. However, further improvement was needed, as, for example, the line intensities in the (6–0) band, though improved by an order of magnitude, are still more than 200% off the experimental values. However, lines in the (7–0) band showed very promising improvement, giving discrepancies within the experimental uncertainty, even better than our best results using the (6220) CAS (see Table VI).

Next, we removed all the problematic points; to avoid leaving the intervals shown in Fig. 2 without any dipole points, we used a sixth-order polynomial to interpolate between regions. We started by fitting all points and then removed problematic points with residues far larger than the standard deviation of the fit. The resulting DMC is represented by this functional form with a standard deviation of about  $10^{-7} e \cdot a_0$ ; its use in intensity calculations is given in the last column of Table V and for all measured (7–0) band lines in the last column of Table III.

### B. Cause of the anomalous *ab initio* points

Removing the bad points resolves our problem with the anomalous transition intensities shown, even though the anomalous points

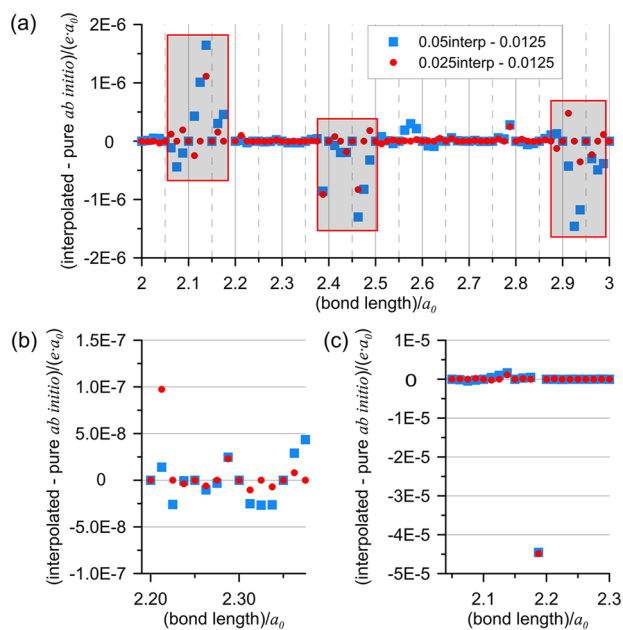


**FIG. 2.** Differences between the *ab initio* dipole moments and ones interpolated from a sparser grid of *ab initio* points. The notations of 0.05, 0.025, and 0.0125 represent different intervals between the *ab initio* points (in  $a_0$ ). The interpolation used cubic-spline functions. (a) Three boxes are used to mark the problematic regions. One outlier at 2.1875  $a_0$  is not displayed. The differences are  $-4.454 \times 10^{-5} e \cdot a_0$  and  $-4.485 \times 10^{-5} e \cdot a_0$  for 0.05–interpolated and 0.025–interpolated points, respectively. (b) Zoom in on the view to show an example of the stable regions. (c) Zoom out the view to show the major outlier of  $-4.5 \times 10^{-5} e \cdot a_0$  at 2.1875  $a_0$ .



**TABLE V.** Calculations with the (7220) CAS and different DMCs. The description of the last four column labels is DF 0.05, 0.025, and 0.0125—steps 0.05, 0.025, and 0.0125; DF 0.0125 removed—step 0.0125 with 1 *ab initio* point removed; fit.ai0125—step 0.0125 data fitted by polynomial expansion. Experimental intensities and wavenumbers for the bands (0–0), (1–0), (2–0), (4–0), and (5–0) are from HITRAN; (3–0) line intensities are from Ref. 3 and wavenumbers are from HITRAN; and (6–0) line intensities are from Ref. 2; and (7–0) intensities are from this work and wavenumbers are from HITRAN. All line intensities are scaled to 100% abundance of  $^{12}\text{C}^{16}\text{O}$ .

| Band | Line | Wavenumber<br>( $\text{cm}^{-1}$ ) | S exp.<br>( $\text{cm molecule}^{-1}$ ) | DF 0.05<br>O–C (%) | DF 0.025<br>O–C (%) | DF 0.0125<br>O–C (%) | DF 0.0125 removed<br>O–C (%) | fit.ai0125<br>O–C (%) |
|------|------|------------------------------------|---|--------------------|---------------------|----------------------|------------------------------|-----------------------|
| 0–0  | R0   | 3.845 03                           | $3.35 \times 10^{-24}$                  | –12.0              | –11.4               | –11.4                | –11.3                        | –11.3                 |
|      | R1   | 7.689 92                           | $2.60 \times 10^{-23}$                  | –12.0              | –11.4               | –11.4                | –11.5                        | –11.3                 |
|      | R2   | 11.534 51                          | $8.37 \times 10^{-23}$                  | –12.0              | –11.4               | –11.4                | –11.4                        | –11.3                 |
| 1–0  | P21  | 2055.400 36                        | $2.54 \times 10^{-20}$                  | –1.6               | –1.0                | –1.0                 | –0.7                         | –0.7                  |
|      | P15  | 2082.002 25                        | $1.45 \times 10^{-19}$                  | –1.6               | –1.0                | –1.0                 | –1.3                         | –1.3                  |
|      | P10  | 2103.269 75                        | $3.30 \times 10^{-19}$                  | –1.6               | –1.0                | –1.0                 | –0.9                         | –0.9                  |
| 2–0  | P40  | 4053.217 40                        | $5.45 \times 10^{-27}$                  | 0.2                | 0.9                 | 0.7                  | 0.7                          | 0.7                   |
|      | P20  | 4170.055 15                        | $2.50 \times 10^{-22}$                  | 0.1                | 0.8                 | 0.7                  | 0.7                          | 0.7                   |
|      | P10  | 4218.485 67                        | $2.39 \times 10^{-21}$                  | 0.1                | 0.8                 | 0.7                  | 1.0                          | 1.0                   |
| 3–0  | P27  | 6210.245 76                        | $7.36 \times 10^{-26}$                  | –0.1               | 0.7                 | 2.7                  | 0.6                          | 0.2                   |
|      | P10  | 6307.287 52                        | $1.37 \times 10^{-23}$                  | 0.1                | 0.8                 | 2.9                  | 0.9                          | 0.5                   |
|      | R10  | 6385.771 47                        | $1.95 \times 10^{-23}$                  | 0.1                | 0.8                 | 2.6                  | 0.7                          | 0.3                   |
| 4–0  | P38  | 8171.272 30                        | $1.24 \times 10^{-31}$                  | –1.7               | –4.4                | 183.8                | –5.9                         | –10.0                 |
|      | P37  | 8180.194 79                        | $2.56 \times 10^{-31}$                  | –1.8               | –4.5                | 170.2                | –5.8                         | –9.7                  |
|      | P22  | 8297.796 94                        | $1.24 \times 10^{-27}$                  | –2.4               | –4.8                | 69.6                 | –6.4                         | –8.4                  |
|      | P10  | 8369.742 87                        | $3.56 \times 10^{-26}$                  | –2.5               | –4.4                | 43.3                 | –5.8                         | –7.0                  |
| 5–0  | P10  | 10 405.920 99                      | $3.18 \times 10^{-28}$                  | 64.1               | 160.2               | –14.2                | 105.5                        | 18.8                  |
|      | P9   | 10 411.334 43                      | $3.24 \times 10^{-28}$                  | 67.9               | 172.1               | –25.6                | 111.9                        | 19.6                  |
|      | P5   | 10 431.249 90                      | $2.37 \times 10^{-28}$                  | 87.6               | 241.5               | –57.3                | 147.0                        | 23.2                  |
|      | R0   | 10 455.892 17                      | $3.62 \times 10^{-29}$                  | 144.0              | 548.1               | –81.9                | 271.0                        | 24.3                  |
| 6–0  | R5   | 12 482.423 74                      | $9.30 \times 10^{-29}$                  | 2733.8             | 1520.4              | –96.9                | 208.9                        | 2.5                   |
|      | R7   | 12 486.956 65                      | $9.33 \times 10^{-29}$                  | 3522.6             | 1878.2              | –97.1                | 227.3                        | 3.8                   |
|      | R9   | 12 490.644 87                      | $7.85 \times 10^{-29}$                  | 4582.3             | 2326.4              | –97.4                | 237.0                        | 1.4                   |
|      | R10  | 12 492.171 85                      | $7.04 \times 10^{-29}$                  | 5476.8             | 2705.6              | –97.5                | 251.1                        | 2.7                   |
| 7–0  | P16  | 14 358.363 21                      | $3.69 \times 10^{-30}$                  | 1807.7             | 73.7                | –70.7                | 0.6                          | 0.0                   |
|      | P13  | 14 380.141 03                      | $6.79 \times 10^{-30}$                  | 1985.5             | 58.9                | –81.8                | –2.1                         | 1.2                   |
|      | P8   | 14 411.573 98                      | $1.11 \times 10^{-29}$                  | 2025.8             | 44.0                | –88.6                | –5.1                         | 2.7                   |
|      | R0   | 14 452.781 45                      | $2.50 \times 10^{-30}$                  | 1969.6             | 37.5                | –90.3                | 7.3                          | 5.6                   |

differ from their correct analog by only about  $10^{-6}$  D; their removal results in a drastic improvement in our results. To determine the cause of these anomalous points, we analyzed the behavior of all stages of our MRCI + Q MOLPRO calculations. It transpired that neither the CAS-self consistent field (SCF) nor the MRCI without Davidson correction or Pople correction<sup>54</sup> produced these anomalies. Performing calculations on a dense grid (100 points per interval from 1.7 to 3.0  $a_0$ ), removing the MRCI values, and retaining just the Davidson correction or Pople correction at each geometry resulted in artificial structures in the curves exactly where we identified problems in Fig. 2, as illustrated in Fig. 3. This showed that these minor corrections to the MRCI calculations are the sole cause of the anomalies.

After identifying the cause of the anomalous points, we performed final tests of the fits of the *ab initio* dipole points. We used the simple polynomial in the following functional form:

$$D(r) = \sum_{k=0}^6 \alpha_k (r - r_0)^k, \quad (1)$$

with only seven parameters  $\alpha_k$ . When we removed only two outliers, the standard deviation of the fit was  $6 \times 10^{-7}$  D. When we removed all problematic points from the fit, the standard deviation was reduced to  $10^{-7}$  D. The results of the intensity calculation practically remained the same. We conclude that to solve the problem with anomalous points, we need to fit the good points with a simple polynomial functional form, as the resulting DMC gives intensities very close to the experimental accuracy for all bands.

We checked many factors that could influence the accuracy of the calculations, including the improvement of the functional form used to represent the DMC. In a series of papers on CO Medvedev and co-workers,<sup>20,21,23–26</sup> they consider the reasons calculated DMCs give anomalously high intensities for overtone lines. However, as

**TABLE VI.** Calculations with the (6220) CAS and different DMCs. The description of the last four column labels: DF and DR denote Davidson fixed and Davidson relaxed corrections of 0.05, 0.025, and grid spacing of 0.05 and  $0.025 a_0$ , respectively. Experimental intensities for the bands (0–0), (1–0), (2–0), (4–0), and (5–0) are from HITRAN; (3–0) line intensities are from Ref. 3; (6–0) line intensities are from Ref. 2; and (7–0) intensities are from this work. All wavenumbers are from HITRAN. All line intensities are scaled to 100% abundance of  $^{12}\text{C}^{16}\text{O}$ .

| Band | Line | Wavenumber<br>( $\text{cm}^{-1}$ ) | S exp.<br>( $\text{cm molecule}^{-1}$ ) | DF 0.05<br>O–C (%) | DF 0.025<br>O–C (%) | DR 0.05<br>O–C (%) | DR 0.025<br>O–C (%) |
|------|------|------------------------------------|---|--------------------|---------------------|--------------------|---------------------|
| 0–0  | R0   | 3.845 03                           | $3.35 \times 10^{-24}$                  | –14.9              | –14.9               | –21.4              | –21.4               |
|      | R1   | 7.689 92                           | $2.60 \times 10^{-23}$                  | –14.9              | –14.9               | –21.4              | –21.4               |
|      | R2   | 11.534 51                          | $8.37 \times 10^{-23}$                  | –14.9              | –14.9               | –21.4              | –21.4               |
| 1–0  | P21  | 2 055.400 36                       | $2.54 \times 10^{-20}$                  | –1.9               | –1.9                | –1.5               | –1.5                |
|      | P15  | 2 082.002 25                       | $1.45 \times 10^{-19}$                  | –1.9               | –1.9                | –1.5               | –1.5                |
|      | P10  | 2 103.269 75                       | $3.30 \times 10^{-19}$                  | –1.9               | –1.9                | –1.5               | –1.5                |
| 2–0  | P40  | 4 053.217 40                       | $5.45 \times 10^{-27}$                  | 0.8                | 0.8                 | 2.2                | 2.2                 |
|      | P20  | 4 170.055 15                       | $2.50 \times 10^{-22}$                  | 0.7                | 0.7                 | 2.0                | 2.0                 |
|      | P10  | 4 218.485 67                       | $2.39 \times 10^{-21}$                  | 0.6                | 0.6                 | 2.0                | 2.0                 |
| 3–0  | P27  | 6 210.245 76                       | $7.36 \times 10^{-26}$                  | 0.8                | 0.8                 | 1.7                | 1.7                 |
|      | P10  | 6 307.287 52                       | $1.37 \times 10^{-23}$                  | 0.8                | 0.9                 | 1.7                | 1.7                 |
|      | R10  | 6 385.771 47                       | $1.95 \times 10^{-23}$                  | 0.7                | 0.7                 | 1.5                | 1.5                 |
| 4–0  | P38  | 8 171.272 30                       | $1.24 \times 10^{-31}$                  | –12.8              | –12.6               | –16.0              | –15.7               |
|      | P37  | 8 180.194 79                       | $2.56 \times 10^{-31}$                  | –12.6              | –12.4               | –15.7              | –15.4               |
|      | P22  | 8 297.796 94                       | $1.24 \times 10^{-27}$                  | –9.7               | –9.6                | –12.0              | –11.8               |
|      | P10  | 8 369.742 87                       | $3.56 \times 10^{-26}$                  | –8.0               | –8.0                | –9.9               | –9.7                |
| 5–0  | P10  | 10 405.920 99                      | $3.18 \times 10^{-28}$                  | 22.6               | 25.2                | 36.6               | 39.9                |
|      | P9   | 10 411.334 43                      | $3.24 \times 10^{-28}$                  | 23.5               | 41.8                | 38.1               | 41.7                |
|      | P5   | 10 431.249 90                      | $2.37 \times 10^{-28}$                  | 28.0               | 31.5                | 46.0               | 50.6                |
|      | R0   | 10 455.892 17                      | $3.62 \times 10^{-29}$                  | 40.0               | 45.4                | 68.0               | 75.7                |
| 6–0  | R5   | 12 482.423 74                      | $9.30 \times 10^{-29}$                  | –1.3               | 9.1                 | –0.7               | 13.7                |
|      | R7   | 12 486.956 65                      | $9.33 \times 10^{-29}$                  | –0.2               | 10.6                | 0.4                | 15.5                |
|      | R9   | 12 490.644 87                      | $7.85 \times 10^{-29}$                  | –2.6               | 8.3                 | –1.8               | 13.3                |
|      | R10  | 12 492.171 85                      | $7.04 \times 10^{-29}$                  | –1.5               | 9.7                 | –0.6               | 14.9                |
| 7–0  | P16  | 14 358.363 21                      | $3.69 \times 10^{-30}$                  | 4.8                | 26.5                | –16.4              | 6.6                 |
|      | P13  | 14 380.141 03                      | $6.79 \times 10^{-30}$                  | 7.3                | 28.4                | –14.8              | 7.8                 |
|      | P8   | 14 411.573 98                      | $1.11 \times 10^{-29}$                  | 10.9               | 31.4                | –12.6              | 9.7                 |
|      | R0   | 14 452.781 33                      | $2.50 \times 10^{-30}$                  | 13.6               | 32.8                | –4.0               | 11.7                |

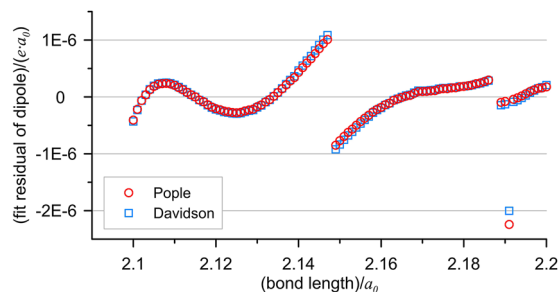
we can see from our *ab initio* calculated intensities, there are no anomalously high values of the intensities of the bands up to the (7–0) band once issues independent of the function form used are resolved. The question of the extrapolation of intensities calculated using a polynomial representation of the DMC to higher overtones will be considered in a subsequent publication on hotlines for all isotopologues of CO.

Table VII gives the coefficients of our power series expansion of the DMC, Eq. (1). Figure 4 compares our *ab initio* dipole moment curve with the semi-empirical curve determined by Medvedev and Ushakov.<sup>26</sup> The two curves are very similar; the DMC of Medvedev

and Ushakov<sup>26</sup> changes sign at a slightly shorter bond length than ours, and the slope of our curve is slightly steeper.

### C. Final results

A comparison between experimental and calculated results for (7–0) band are shown in Fig. 5. Recently, Fan *et al.*<sup>55</sup> used a different, algebraic approach to calculate line intensities, including three lines P23, P63, and P103 of the (7–5) band of CO at two temperatures of 296 and 3000 K. Our calculations with the fit.ai0125 model agree with these values by about 1%.



**FIG. 3.** Fit residuals of the DMCs with Pople correction and Davidson correction using a sixth order polynomial function in the bond length range of 2.1–2.2  $a_0$ . Note that there are two major outliers for Pople corrections, which are both  $-4.1 \times 10^{-5} e \cdot a_0$  at 2.187  $a_0$  and 2.188  $a_0$ , and the other two outliers for Davidson corrections are  $-4.5 \times 10^{-5} e \cdot a_0$  also at 2.187  $a_0$  and 2.188  $a_0$ . These outliers were found in the test polynomial fit and were excluded from the final six-order polynomial fit.

**TABLE VII.** Coefficients of the power series expansion from Eq. (1) of the DMC of CO ( $\alpha_k$  in a.u.).

| $r_0$      | $2.2a_0$       |
|------------|----------------|
| $\alpha_0$ | -0.006 350 502 |
| $\alpha_1$ | 0.659 122 01   |
| $\alpha_2$ | -0.049 959 1   |
| $\alpha_3$ | -0.135 641     |
| $\alpha_4$ | 0.038 216      |
| $\alpha_5$ | 0.014 599      |
| $\alpha_6$ | -0.011 909     |

A bigger challenge is to construct an *ab initio* DMC for CO capable predicting intensities within experimental uncertainty using a single model for all the bands. The last column of Table V shows that we are already close to the solution; indeed, we are the closest yet. In particular, all the line intensities presented in Table V differ from the experimental values to not more than about 2–5 times the experimental uncertainty.

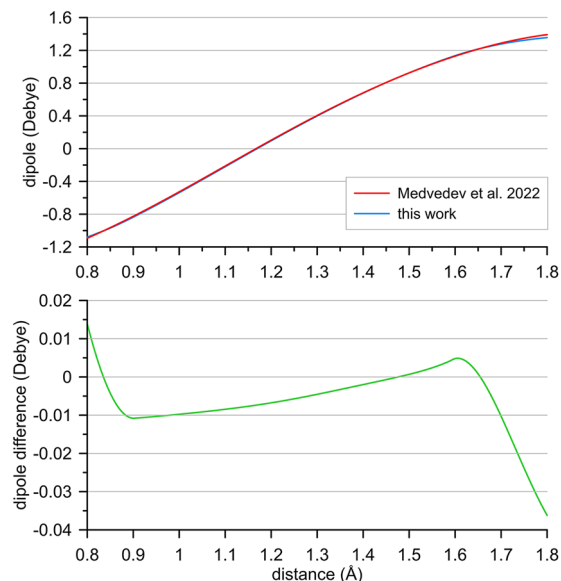


**FIG. 4.** Top panel: comparison of CO dipole curves computed *ab initio* in this work—fit.ai0125 (blue) and determined semi-empirically by Medvedev and Ushakov<sup>26</sup> (red). Bottom panel: the difference, this work—Medvedev and Ushakov's,<sup>26</sup> curves.

Let us discuss briefly how the results shown in the last column of Table V compare with the experimental uncertainty of the corresponding CO bands. The pure rotational spectrum is anomalously weak and up to five orders of magnitude weaker than the usual rotational spectrum of many diatomic molecules; the 11% difference from the HITRAN data is a result of this anomalous weakness. This discrepancy requires very accurate calculations and a separate study focusing on tiny corrections. The intensities of the fundamental (1–0) and overtone (2–0) bands are not known experimentally with reliable sub-percent accuracy, so our calculations show acceptable agreement with the measurements. The calculated intensities for the (3–0) and (4–0) bands are about five times worse than the experimental accuracies, 0.1% and 2%, respectively. The (5–0) band

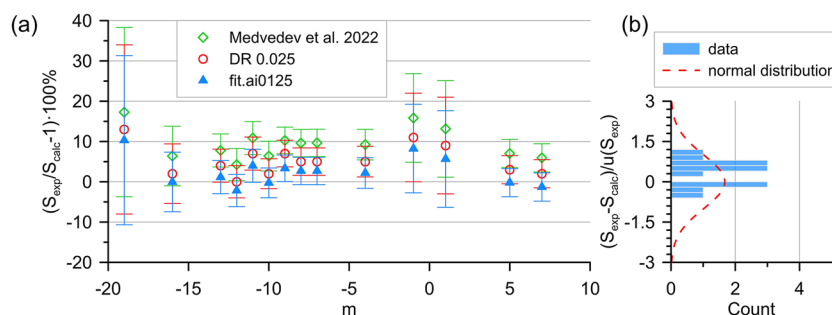


**FIG. 5.** (a) Calculated line intensities for the CO (7–0) band compared to the measured ones vs the quantum number  $m$ , where  $m = -J$  for the P branch transitions and  $m = J + 1$  for the R branch, and  $J$  is the lower-state rotational quantum number, together with data by Medvedev and Ushakov.<sup>26</sup> (b) Histogram of differences between observed and calculated (fit.ai0125) line intensities in units of standard experimental uncertainty,  $(S_{\text{exp}} - S_{\text{calc}})/u(S_{\text{exp}})$ , and corresponding normal distribution.

line intensities are only known approximately, with an uncertainty of 30%–40%,<sup>2</sup> so a 20% discrepancy in the calculations is acceptable. The observed minus calculated (6–0) band line intensities are about double the experimental uncertainties of 2% for this band.<sup>2</sup> Thus, a several-fold improvement in the accuracy of the calculated line intensities is needed for most of the bands. Thus, the conclusion is that the overall predicted intensities for all the bands have never been so good, but a complete solution requires more work.

#### IV. CONCLUSIONS

Lines in the (7–0) high overtone band of CO are observed, and their intensities are measured and calculated using an *ab initio* model for the dipole moment curve. This is the first measurement of intensities in the optical region of such weak lines with such a high accuracy. Our final calculations give line intensities within the estimated experimental uncertainties. The theoretical part of this paper clearly demonstrates two things: first, the importance of accurate and reliable knowledge of the line intensities to address the yet unsolved problem of accurate calculation of intensities for all rovibrational bands, including overtones, belonging to a particular molecule. We have clearly advanced the solution to this problem significantly in this work.

That brings us to the second feature of the theoretical part of this paper. Our initial calculations gave absurdly high discrepancies between our *ab initio* calculated and experimentally measured line intensities for (7–0) overtone transitions when we used the potentially very accurate model developed in our previous study of the (3–0) overtone.<sup>3</sup> Inspired by the high accuracy of the experimental data obtained in the present work, we managed to come very close to calculating the intensities for all bands of CO with experimental accuracy using a single model. The reason for the initial forty-fold discrepancy turned out to be very small deviations Davidson or the Pople corrections to the MRCI dipole moment calculations. Further steps leading to a complete solution of the problem of the calculation of line intensities for all bands within experimental error became clear during the work on this paper and will be a subject of immediate future work.

#### ACKNOWLEDGMENTS

The reported study was funded by RFBR under Research Project Nos. 18-02-00705 and 18-32-00698. The research conducted at NCU was supported by National Science Centre Poland, Project Nos. 2015/18/E/ST2/00585, 2018/30/E/ST2/00864, 2018/29/B/ST2/02974, and 2021/42/E/ST2/00152, and it was part of the program of the National Laboratory FAMO in Toruń, Poland. This work was supported by the European Research Council (ERC) under the European Union's Horizon 2020 research and innovation program through Advance Grant No. 883830 and by the UK NERC through grant NE/T000767/1. N.F.Z. and O.L.P. acknowledge the support by State Project IAP RAS No. 0030-2021-0016. O.L.P. is grateful to Nino Ipran for his technical support. G.L. acknowledges the technical support from Gert Lindner for using the PTB Linux Cluster. G.L. is grateful to Prof. Ravi Fernandes for acquiring the Molpro license.

#### AUTHOR DECLARATIONS

##### Conflict of Interest

The authors have no conflicts to disclose.

##### Author Contributions

**Aleksandr A. Balashov:** Data curation (equal); Formal analysis (equal); Investigation (equal); Software (equal); Visualization (equal); Writing – review & editing (equal). **Katarzyna Bielska:** Conceptualization (equal); Data curation (equal); Funding acquisition (equal); Investigation (equal); Visualization (equal); Writing – original draft (equal). **Gang Li:** Data curation (equal); Investigation (equal); Visualization (equal); Writing – original draft (equal). **Aleksandra A. Kyuberis:** Investigation (equal). **Szymon Wójtewicz:** Funding acquisition (equal); Investigation (equal); Validation (equal); Writing – review & editing (equal). **Jolanta Domysławska:** Formal analysis (equal); Funding acquisition (equal); Investigation (equal); Validation (equal); Visualization (equal); Writing – review & editing (equal). **Roman Ciuryło:** Methodology (equal); Validation (equal); Writing – review & editing (equal). **Nikolay F. Zobov:** Formal analysis (equal); Investigation (equal); Methodology (equal); Visualization (equal). **Daniel Lisak:** Conceptualization (equal); Funding acquisition (equal); Methodology (equal); Supervision (equal); Validation (equal); Writing – review & editing (equal). **Jonathan Tennyson:** Conceptualization (equal); Funding acquisition (equal); Writing – review & editing (equal). **Oleg L. Polyansky:** Conceptualization (equal); Formal analysis (lead); Funding acquisition (equal); Methodology (lead); Writing – original draft (equal).

#### DATA AVAILABILITY

The data that support the findings of this study are available within the article.

#### REFERENCES

- S. Wójtewicz, K. Stec, P. Masłowski, A. Cygan, D. Lisak, R. S. Trawiński, and R. Ciuryło, *J. Quant. Spectrosc. Radiat. Transfer* **130**, 191–200 (2013).
- G. Li, I. E. Gordon, L. S. Rothman, Y. Tan, S.-M. Hu, S. Kassi, A. Campargue, and E. S. Medvedev, *Astrophys. J., Suppl. Ser.* **216**, 15 (2015).
- K. Bielska, A. A. Kyuberis, Z. D. Reed, G. Li, A. Cygan, R. Ciuryło, D. Lisak, E. M. Adkins, L. Lodi, J. T. Hodges *et al.*, *Phys. Rev. Lett.* **129**, 043002 (2022).
- I. I. Mizus, L. Lodi, J. Tennyson, N. F. Zobov, and O. L. Polyansky, *J. Mol. Spectrosc.* **386**, 111621 (2022).
- A. W. Mantz and J.-P. Maillard, *J. Mol. Spectrosc.* **53**, 466 (1974).
- D. N. B. Hall, *Astrophys. J.* **182**, 977 (1973).
- N. M. Förster Schreiber, *Astron. J.* **120**, 2089 (2000).
- M. G. Berthoud, L. D. Keller, T. L. Herter, M. J. Richter, and D. G. Whelan, *Astrophys. J.* **660**, 461 (2007).
- F. Martins, M. Pomarès, L. Deharveng, A. Zavagno, and J. C. Bouret, *Astron. Astrophys.* **510**, A32 (2010).
- GRAVITY collaboration, A. Caratti o Garatti, R. Fedriani, R. Garcia Lopez, M. Koutoulaki, K. Perraut, H. Linz, W. Brandner, P. Garcia, L. Klarmann, T. Henning *et al.*, *Astron. Astrophys.* **635**, L12 (2020).
- Á. Kóspál, P. Ábrahám, M. Goto, Z. Regály, C. P. Dullemond, T. Henning, A. Juhász, A. Sicilia-Aguilar, and M. van den Ancker, *Astrophys. J.* **736**, 72 (2011).

- <sup>12</sup>T. Geballe, URL [www.gemini.edu/observing/resources/near-ir-resources/spectroscopy/co-lines-and-band-heads#Head](http://www.gemini.edu/observing/resources/near-ir-resources/spectroscopy/co-lines-and-band-heads#Head).
- <sup>13</sup>T. Zelevinsky, S. Kotochigova, and J. Ye, *Phys. Rev. Lett.* **100**, 043201 (2008).
- <sup>14</sup>F. Oyafuso, V. H. Payne, B. J. Drouin, V. M. Devi, D. C. Benner, K. Sung, S. Yu, I. E. Gordon, R. Kochanov, Y. Tan, D. Crisp, E. J. Mlawer, and A. Guillaume, *J. Quant. Spectrosc. Radiat. Transfer* **203**, 213 (2017).
- <sup>15</sup>L. Lodi, J. Tennyson, and O. L. Polyansky, *J. Chem. Phys.* **135**, 034113 (2011).
- <sup>16</sup>O. L. Polyansky, K. Bielska, M. Ghysels, L. Lodi, N. F. Zobov, J. T. Hodges, and J. Tennyson, *Phys. Rev. Lett.* **114**, 243001 (2015).
- <sup>17</sup>T. A. Odintsova, E. Fasci, L. Moretti, E. J. Zak, O. L. Polyansky, J. Tennyson, L. Gianfrani, and A. Castrillo, *J. Chem. Phys.* **146**, 244309 (2017).
- <sup>18</sup>P. Tans and P. Zellweger, GAW Report No. 229, World Meteorological Organization, 2016.
- <sup>19</sup>S. N. Yurchenko, J. Tennyson, J. Bailey, M. D. J. Hollis, and G. Tinetti, *Proc. Natl. Acad. Sci. U. S. A.* **111**, 9379 (2014).
- <sup>20</sup>V. V. Meshkov, A. Y. Ermilov, A. V. Stolyarov, E. S. Medvedev, V. G. Ushakov, and I. E. Gordon, *J. Quant. Spectrosc. Radiat. Transfer* **280**, 108090 (2022).
- <sup>21</sup>E. S. Medvedev and V. G. Ushakov, *J. Quant. Spectrosc. Radiat. Transfer* **272**, 107803 (2021).
- <sup>22</sup>E. S. Medvedev, *J. Chem. Phys.* **137**, 174307 (2012).
- <sup>23</sup>E. S. Medvedev, V. V. Meshkov, A. V. Stolyarov, V. G. Ushakov, and I. E. Gordon, *J. Mol. Spectrosc.* **330**, 36 (2016).
- <sup>24</sup>E. S. Medvedev, V. G. Ushakov, A. V. Stolyarov, and I. E. Gordon, *J. Chem. Phys.* **147**, 164309 (2017).
- <sup>25</sup>E. S. Medvedev and V. G. Ushakov, *J. Mol. Spectrosc.* **349**, 60 (2018).
- <sup>26</sup>E. S. Medvedev and V. G. Ushakov, *J. Quant. Spectrosc. Radiat. Transfer* **288**, 108255 (2022).
- <sup>27</sup>K. Bielska, J. Domysławska, S. Wójtewicz, A. Balashov, M. Słowiński, M. Piwiński, A. Cygan, R. Ciuryło, and D. Lisak, *J. Quant. Spectrosc. Radiat. Transfer* **276**, 107927 (2021).
- <sup>28</sup>J. T. Hodges, H. P. Layer, W. W. Miller, and G. E. Scace, *Rev. Sci. Instrum.* **75**, 849 (2004).
- <sup>29</sup>R. W. P. Drever, J. L. Hall, F. V. Kowalski, J. Hough, G. M. Ford, A. J. Munley, and H. Ward, *Appl. Phys. B* **31**, 97 (1983).
- <sup>30</sup>A. Cygan, D. Lisak, P. Masłowski, K. Bielska, S. Wójtewicz, J. Domysławska, R. S. Trawiński, R. Ciuryło, H. Abe, and J. T. Hodges, *Rev. Sci. Instrum.* **82**, 063107 (2011).
- <sup>31</sup>A. Cygan, P. Wcisło, S. Wójtewicz, P. Masłowski, J. T. Hodges, R. Ciuryło, and D. Lisak, *Opt. Express* **23**, 14472 (2015).
- <sup>32</sup>J. Domysławska, S. Wójtewicz, D. Lisak, A. Cygan, F. Ozimek, K. Stec, C. Radzewicz, R. S. Trawiński, and R. Ciuryło, *J. Chem. Phys.* **136**, 024201 (2012).
- <sup>33</sup>A. Cygan, S. Wójtewicz, G. Kowzan, M. Zaborowski, P. Wcisło, J. Nawrocki, P. Krehlik, Ł. Śliwczyński, M. Lipiński, P. Masłowski, R. Ciuryło, and D. Lisak, *J. Chem. Phys.* **144**, 214202 (2016).
- <sup>34</sup>P. R. Berman, *J. Quant. Spectrosc. Radiat. Transf.* **12**, 1331 (1972).
- <sup>35</sup>F. Rohart, H. Mäder, and H. W. Nicolaisen, *J. Chem. Phys.* **101**, 6475 (1994).
- <sup>36</sup>R. H. Dicke, *Phys. Rev.* **89**, 472 (1953).
- <sup>37</sup>D. Priem, F. Rohart, J.-M. Colmont, G. Włodarczyk, and J.-P. Bouanich, *J. Mol. Struct.* **517-518**, 435 (2000).
- <sup>38</sup>R. Ciuryło and J. Szudy, *J. Quant. Spectrosc. Radiat. Transfer* **57**, 411 (1997).
- <sup>39</sup>S. Wójtewicz, A. Cygan, P. Masłowski, J. Domysławska, D. Lisak, R. S. Trawiński, and R. Ciuryło, *J. Quant. Spectrosc. Radiat. Transfer* **144**, 36 (2014).
- <sup>40</sup>B. Lance, G. Blanquet, J. Walrand, and J.-P. Bouanich, *J. Mol. Spectrosc.* **185**, 262 (1997).
- <sup>41</sup>A. S. Pine, *J. Quant. Spectrosc. Radiat. Transfer* **62**, 397 (1999).
- <sup>42</sup>N. H. Ngo, D. Lisak, H. Tran, and J.-M. Hartmann, *J. Quant. Spectrosc. Radiat. Transfer* **129**, 89 (2013).
- <sup>43</sup>N. H. Ngo, D. Lisak, H. Tran, and J.-M. Hartmann, *J. Quant. Spectrosc. Radiat. Transfer* **134**, 105 (2014).
- <sup>44</sup>J. Tennyson, P. F. Bernath, A. Campargue, A. G. Császár, L. Daumont, R. R. Gamache, J. T. Hodges, D. Lisak, O. V. Naumenko, L. S. Rothman *et al.*, *Pure Appl. Chem.* **86**, 1931 (2014).
- <sup>45</sup>D. C. Benner, C. P. Rinsland, V. M. Devi, M. A. H. Smith, and D. Atkins, *J. Quant. Spectrosc. Radiat. Transfer* **53**, 705 (1995).
- <sup>46</sup>A. S. Pine and R. Ciuryło, *J. Mol. Spectrosc.* **208**, 180 (2001).
- <sup>47</sup>J. Domysławska, S. Wójtewicz, P. Masłowski, K. Bielska, A. Cygan, M. Słowiński, R. S. Trawiński, R. Ciuryło, and D. Lisak, *J. Quant. Spectrosc. Radiat. Transfer* **242**, 106789 (2020).
- <sup>48</sup>J. A. Coxon and P. G. Hajigeorgiou, *Can. J. Phys.* **70**, 40 (1992).
- <sup>49</sup>J. A. Coxon and P. G. Hajigeorgiou, *J. Chem. Phys.* **121**, 2992 (2004).
- <sup>50</sup>H.-J. Werner, P. J. Knowles, F. R. Manby, J. A. Black, K. Doll, A. Heßelmann, D. Kats, A. Köhn, T. Korona, D. A. Kreplin *et al.*, *J. Chem. Phys.* **152**, 144107 (2020).
- <sup>51</sup>S. R. Langhoff and E. R. Davidson, *Int. J. Quantum Chem.* **8**, 61–72 (1974).
- <sup>52</sup>I. E. Gordon, L. S. Rothman, R. J. Hargreaves, R. Hashemi, E. V. Karlovets, F. M. Skinner, E. K. Conway, C. Hill, R. V. Kochanov, Y. Tan *et al.*, *J. Quant. Spectrosc. Radiat. Transf.* **277**, 107949 (2022).
- <sup>53</sup>E. K. Conway, A. A. Kyuberis, O. L. Polyansky, J. Tennyson, and N. F. Zobov, *J. Chem. Phys.* **149**, 084307 (2018).
- <sup>54</sup>J. A. Pople, R. Seeger, and R. Krishnan, *Int. J. Quantum Chem. Symp.* **12**, 149–163 (1977).
- <sup>55</sup>Z. Fan, J. He, Z. Ni, Q. Fan, J. Fu, Y. Xu, H. Li, J. Ma, and F. Xie, *Spectrochim. Acta, Part A* **264**, 120278 (2022).